(NASA-CR-130114) ADVANCED FIGURE SENSOR Final Report H.J. Robertson (Perkin-Elmer Corp.) 15 Mar. 1972 43 p CSCL 14B

N73-12454

Unclas

G3/14 48358

PERKIN-ELMER

PERKIN-ELMER

OPTICAL GROUP NORWALK, CONNECTICUT

ENGINEERING REPORT NO. 11008

ADVANCED FIGURE SENSOR

FINAL REPORT

DATE: 15 MARCH 1972

PREPARED FOR: NATIONAL AERONAUTICS AND SPACE ADMINISTRATION

GODDARD SPACE FLIGHT CENTER

GLEN DALE ROAD

GREENBELT, MARYLAND 20771

Contract No.: NAS 5-21546
Project No.: SPO 33018

PREPARED BY: Hugh J. Robertson
Hugh J. Robertson, Project Manager

APPROVED BY: D J McCarthy
Daniel J. McCarthy, Manager,
Scientific Payloads Department

REF

TABLE OF CONTENTS

LIST OF ILLUSTRATIONS

1.0 SUMMARY

The Advanced Figure Sensor Study performed by Perkin-Elmer under NASA Contract No. NAS 12-681 (Phase I) examined approaches for measuring parabolic mirror surfaces. This contract (Phase II) extended that effort with the specific purpose of constructing a working model of the Advanced Figure Sensor.

All major technical developments were documented during the previous NASA contract. This report deals only with the final test results obtained from the working model of the Advanced Figure Sensor. It also describes the construction of the unit.

1.1 SCOPE

The major goal of this program was to construct a working model of the Advanced Figure Sensor based on the techniques and components developed during Phase I, NASA Contract NAS 12-681. The key technical performance goals of this project were:

- Accuracy: The systematic error goal of the figure sensor to be ± 1/100 wavelength after calibration.
- Electronic Stability: Random time - varying fluctuations of the figure sensor to be less than 1/200 wavelengths rms.
- Resolution and Range: From 1/100 fringe to a goal of 100 fringes across the aperture.
- Response Speed: To accomodate thermal distortion rates, a need for a frame rate of one frame in ten seconds is anticipated.

The optical-electrical arrangement developed and proposed during Phase I of the figure sensor project is shown in Figure 1. Key elements in

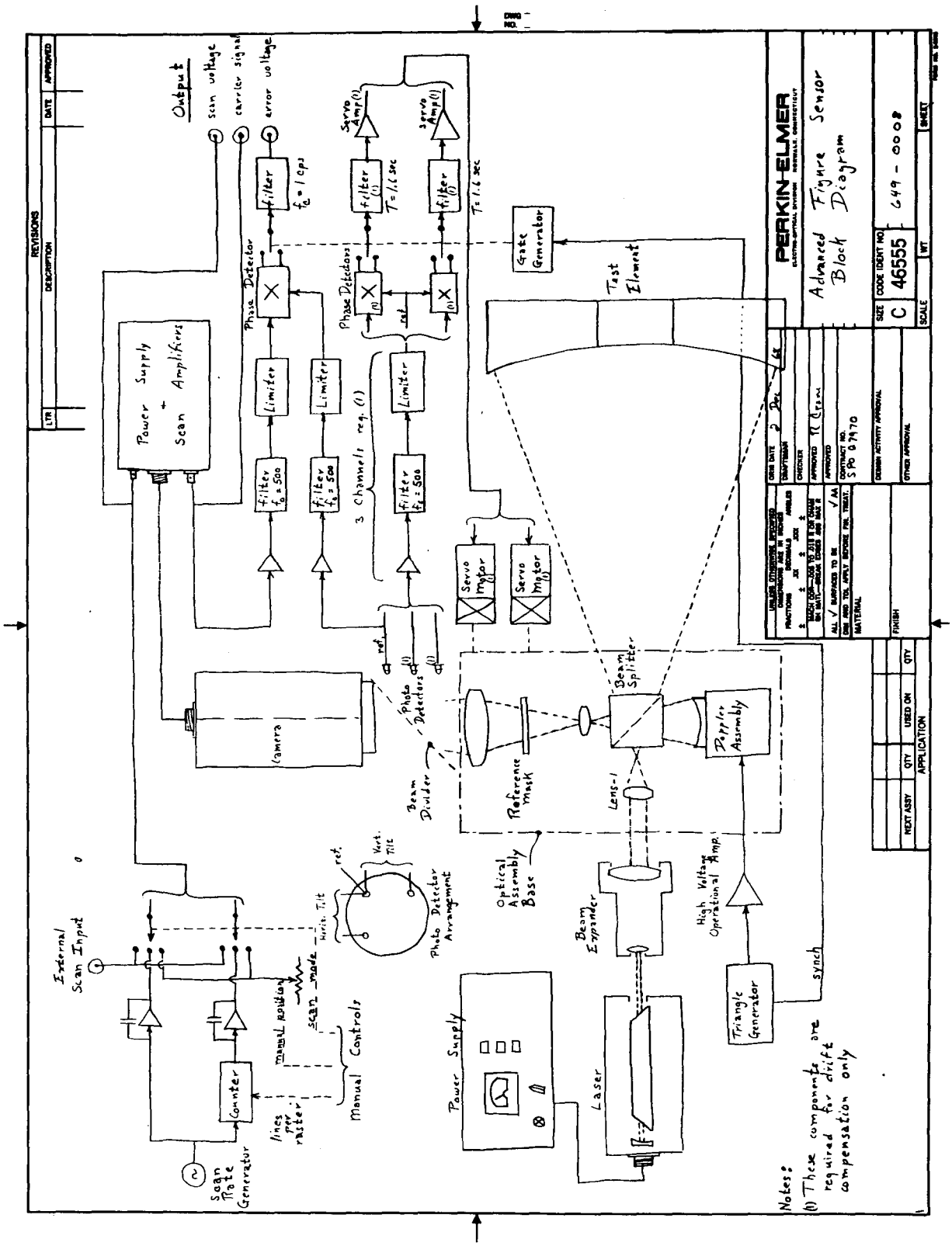

Figure 1. Advanced Figure Sensor Block Diagram
(Contract No. NAS 12-681)

this approach were the Perkin-Elmer 5800 Laser, ITT F5005 Image Dissector, Doppler Frequency Shifter with overall hardware emphasis placed on achieving an instrument that was space qualifiable. To this end, solid-state electronics were used throughout the instrument; space qualifiable peristaltic actuators were considered in the initial design, and mounting provisions for these were incorporated in the figure sensor. Due to reliability problems encountered with the peristaltic actuator prototypes (see contract supplemental agreement no. 2), an arrangement using a stepper motor to drive a differential linkage was actually used to provide drives for the thermal compensating mount. Materials were carefully selected, and, where possible, mechanisms were designed with parts that avoided rubbing surfaces of similar materials. The thermal x-y translating mount, for instance, achieves linear motion using flexure blades in a parallelogram arrangement.

1.2 TECHNICAL APPROACH

The final system design used for the working model of the Advanced Figure Sensor is shown in the block diagram of Figure 2. A modified Twyman-Green interferometer is used for measuring test mirror surface errors. This is a two-beam interferometer that uses a 6328Å Perkin-Elmer laser for a light source, a F5005 ITT Image Dissector for figure error readout, and photodiodes to detect test mirror tilt at the fringe plane.

The optical layout includes an optically bonded 32mm cube beamsplitter which divides the incoming laser beam into two plane wavefronts. A one-inch optical flat is used as a reference surface in one path, and an aspherical decollimating lens forms a spherical wavefront which is reflected from the mirror under test in the other path.

The interferometric output fringe pattern exiting the 32mm cube beamsplitter, derived by comparing the reflected reference mirror wavefront with the reflected test mirror wavefront, is projected onto both the photodiode array and the image dissector by means of a 70/30 percent beam divider.

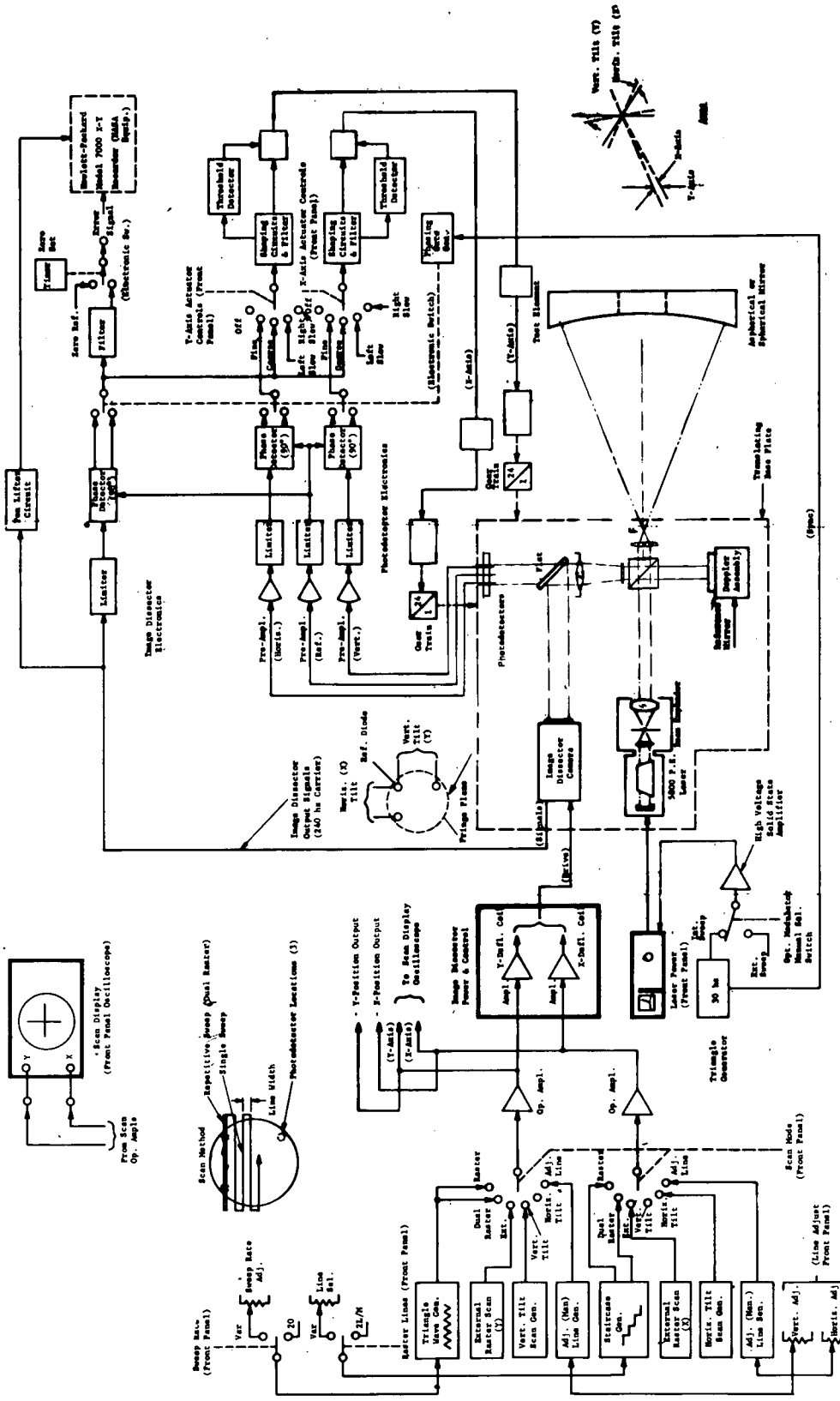

Figure 2. Complete System Block Diagram

The usable (linear portion) of the image dissector is 80 percent of the full 1.10-inch aperture of 0.88-inch. The relaying optics were designed to image the clear aperture of the test mirror onto the usable (0.88-inch) image dissector aperture.

The mechanical translating solid-state Doppler frequency shifter uses piezoelectric elements to translate the spherical reference mirror through a range of 8 to 12 fringes, accounting for both the forward and reverse directions. This translation varies the reference mirror path length relative to the test mirror path length. An optical path length variation between the two interferometer paths is the same as an optical phase shift between the two paths, which causes the fringe pattern to alternate in intensity. A pair of photodiodes (or the image dissector and one diode) spaced apart in the fringe plane and each sensing a set of interfering rays, will produce electrical output signals that vary as the optical phase shift varies. The signal variation is sinusoidal for linear motions of the frequency shifter. The two photodiode outputs are compared electrically and the relative phase shift between the two output signals becomes a measure of the surface error on the test mirror. By definition, a figure error on the test mirror is a relative optical path length difference between a perfect reference mirror and an imperfect test mirror surface. The electrical phase shifts representing the figure errors are converted into DC output voltages by phase detector or demodulator circuits. The conversion is accomplished by electrical multiplication of the photodiode signal output with the reference photodiode signal output. Since the photodiode outputs are sinusoidal, sidebands result from the multiplication, at twice the carrier frequency, but these components are eliminated by filtering, leaving only the term proportional to the phase shift between the two signals.

A major subsystem development not undertaken during Phase I of the Advanced Figure Sensor Project but included in this phase was the design, fabrication, and test of a two-axis thermal compensating mount. The mount equips the figure sensor with two translational axes to compensate for test

mirror tilt relative to the figure sensor. Each axis of the thermal mount is driven by a stepper motor actuator operating through a 100:1 linkage. The actuators are operated from amplifiers which generate a sequence of pulses and the electrical commands for these amplifiers are obtained from the photodiode sensors and associated phase detector electronics.

In order to aid in initially aligning the figure sensor to the test mirror, a manual adjustment stand was designed and incorporated as part of the figure sensor hardware. The adjustment stand has five separate degrees of freedom, three translation (x,y, and z) and two angular axes. All adjustable motions are referenced to the optical axis of the figure sensor.

1.3 SUMMARY OF RESULTS

Significant technical advancements were accomplished during the development of the working model of the figure sensor. A flexure blade, two-axis, thermal compensating mount was developed for maintaining figure sensor alignment during changing thermal gradients. Motor driven actuators are used in conjunction with a 100:1 linkage which enable the figure sensor optical base to be positioned to steps equivalent to $\lambda/400$ tilt in an open-loop configuration for an f/2.5 mirror. The thermal mount closed-servo configuration is capable of nulling the tilt angles of the test mirror to less than 1/100 (peak) wavelengths, which is an equivalent test mirror tilt angle of less than 0.0003 arc-seconds for a 20-inch diameter mirror.

The spatial resolution of the image dissector was measured at 0.005 to 0.006 inch. This type of resolution is the equivalent of nearly 200 fringes across the clear aperture of the mirror.

Errors of $\lambda/100$ peak could be detected and measured after calibration, based on noise output measurements, stability measurements, and tilt control. The output noise level and stability of the photodiode phase detector circuits was measured at less than $\lambda/200$ rms and the image dissector output was also measured at less than $\lambda/200$ rms.

Repeatability measurements using raster scans resulted in occasional errors of $\lambda/40$ to $\lambda/80$ peak, but the majority (95 percent) of these errors were smaller than $\lambda/80$ peak. Such measurements included retraces of raster scans with up to 30 minute intervals between runs.

2.0 DETAILED DESCRIPTION OF THE WORKING MODEL

A photograph of the working model of the figure sensor is shown in Figure 3. It consists of the figure sensor assembly, the manual adjustment stand, and the control console.

All the control electronics, power supplies, and instrumentation are packaged in the control console. The components located inside the figure sensor assembly include the ITT F5005 Image Dissector, the Doppler frequency shifter, the thermal compensators, and the optics. The figure sensor assembly is designed with front and rear covers to provide easy access to all parts of the instrument. The detailed design of the figure sensor and console is described in the following paragraphs. The mechanical layout drawing for the instrument is presented in Figure 4.

2.1 OPTICAL/MECHANICAL CONSTRUCTION

The construction and mechanical operation of the figure sensor assembly and manual adjustment stand are described below.

2.1.1 Thermal Compensating Mount: The thermal compensating mount was designed for the purpose of automatically correcting for two-axis angular tilt of the test mirror caused by thermal drifts. Since a test mirror tilt is, for all practical purposes, identical to a translation at the figure sensor assembly, thermal control was accomplished by translating the figure sensor optical base in two axes using a flexure blade parallelogram.

A partial assembly of the figure sensor is shown in Figure 5 illustrating the type of construction used for the thermal mount. The main optical base is suspended on four flexure blades, which allows it to translate ± 0.01-inch horizontally. The opposite ends of the inner flexure blades are fastened to an intermediate box-like structure. This intermediate structure is, in turn, supported by four outer flexure blades that allow it to be translated vertically by ± 0.01-inch, thus translating the optical base in a vertical direction.

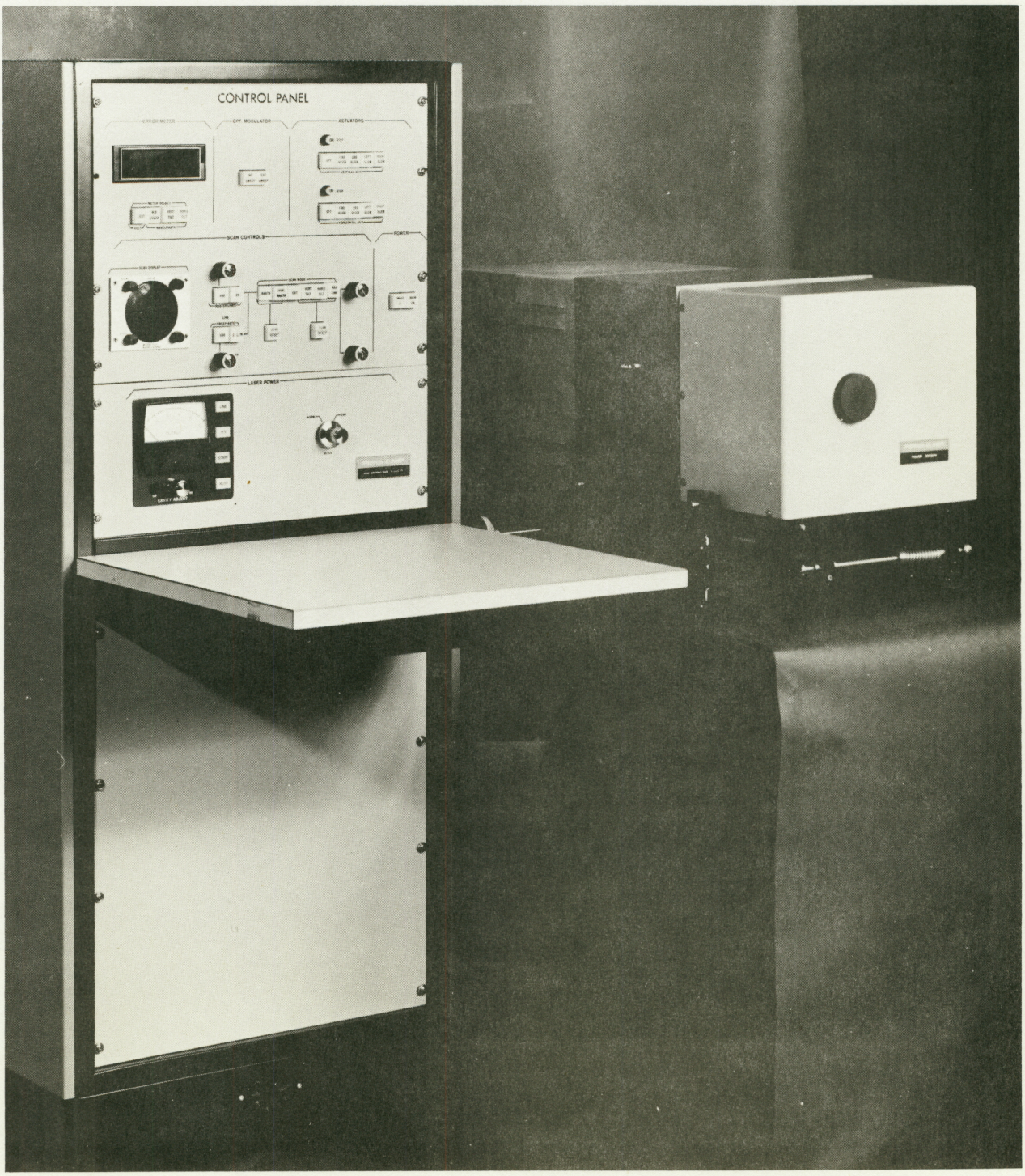

Figure 3. Working Model of the Advanced Figure Sensor

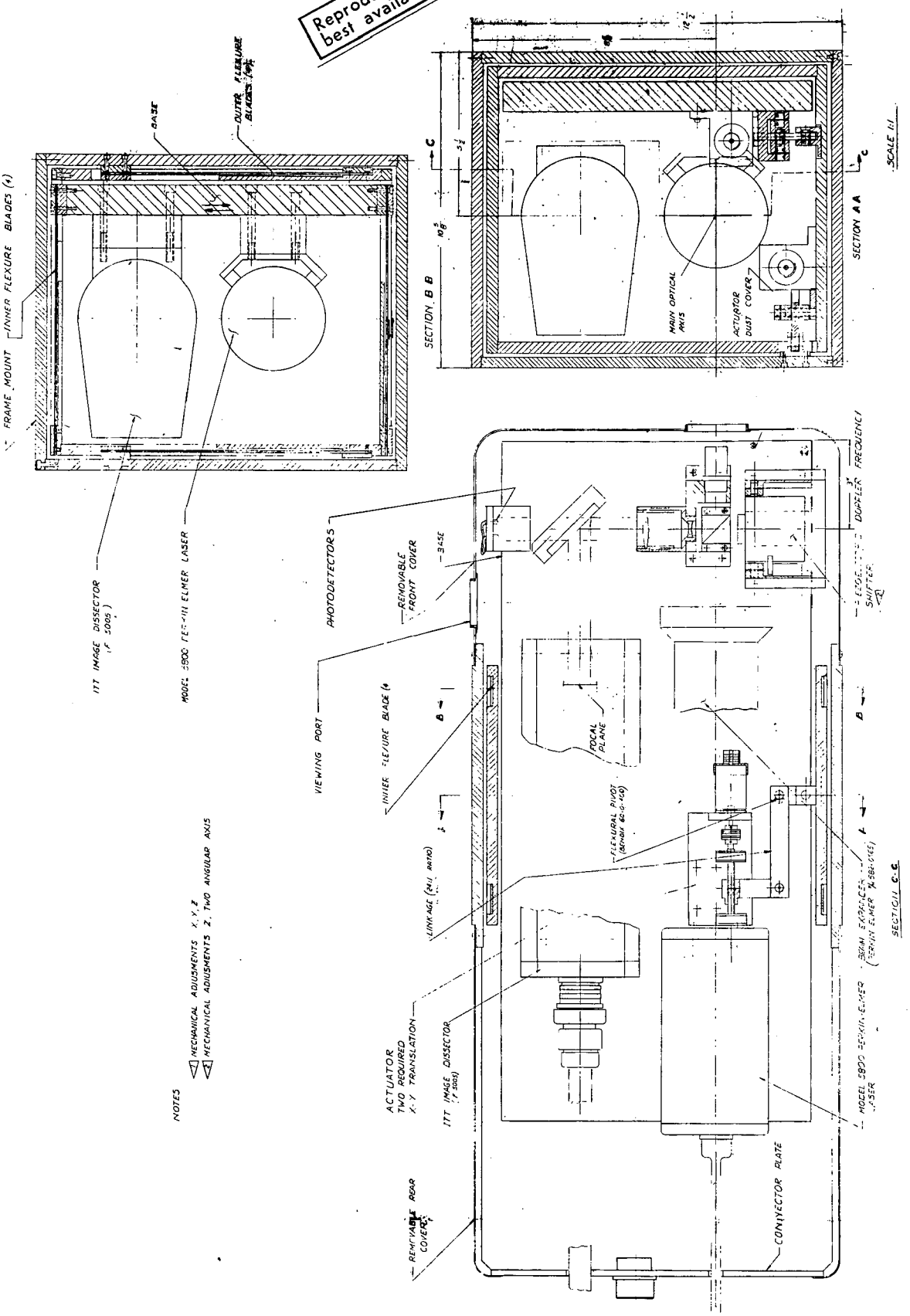

Figure 4. Figure Sensor Mechanical Layout Drawing

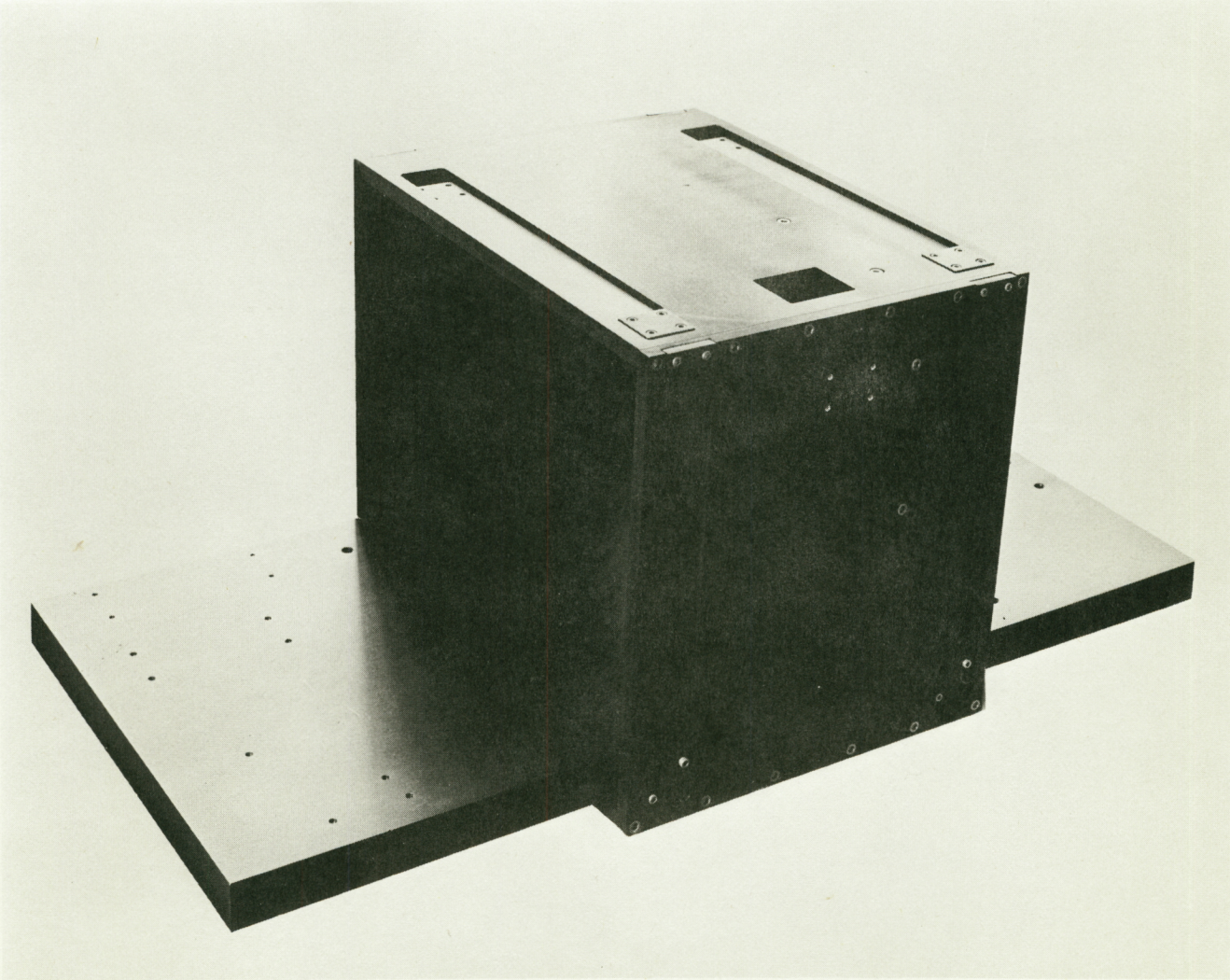

Figure 5. Flexure Blade Parallogram Partial Assembly (One Axis)

The opposite ends of the outer flexure blades are then attached to the main frame of the figure sensor.

Figure 6 shows one of the actuator subassemblies that are used to drive each axis of the thermal compensating mount. Each actuator drives through a 100:1 flexure bearing linkage (see mechanical layout drawing, Figure 4). The purpose of the linkages is to reduce the displacement of the optical base per motor step. In addition, the optical base with all components added weighs 50 pounds and when the figure sensor assembly is mounted horizontally, as shown in Figure 3, this weight must be counteracted in the vertical direction. The 100:1 linkage reduces this load to 1/2 pound as seen at the vertical actuator.

2.1.2 Optical Base: All the interferometer components are mounted on a common one-inch thick aluminum baseplate, in order to assure that the optical/mechanical alignment is maintained. Figure 7 is a photograph of the optical base layout front and rear showing the Perkin-Elmer model 5800 laser, image dissector, photodiodes, Doppler frequency shifter, and optical elements. The 32mm beamsplitter is bonded to a 1/8-inch titanium piece that, in turn, is fastened to a center aluminum mounting block. The laser f/5 decollimating lens and the mirror imaging lens are mounted to the same block. Various reference surfaces on this center mounting block are used for alignment.

2.1.3 Image Dissector: The ITT F5005 Image Dissector has a 1.10-inch aperture which is linear over 80 percent of its diameter. It uses a 0.0015-inch scanning aperture with an S-20 photocathode surface which has high sensitivity at 6328Å. Further details concerning this unit are available in the ITT Vidissector operation manual.

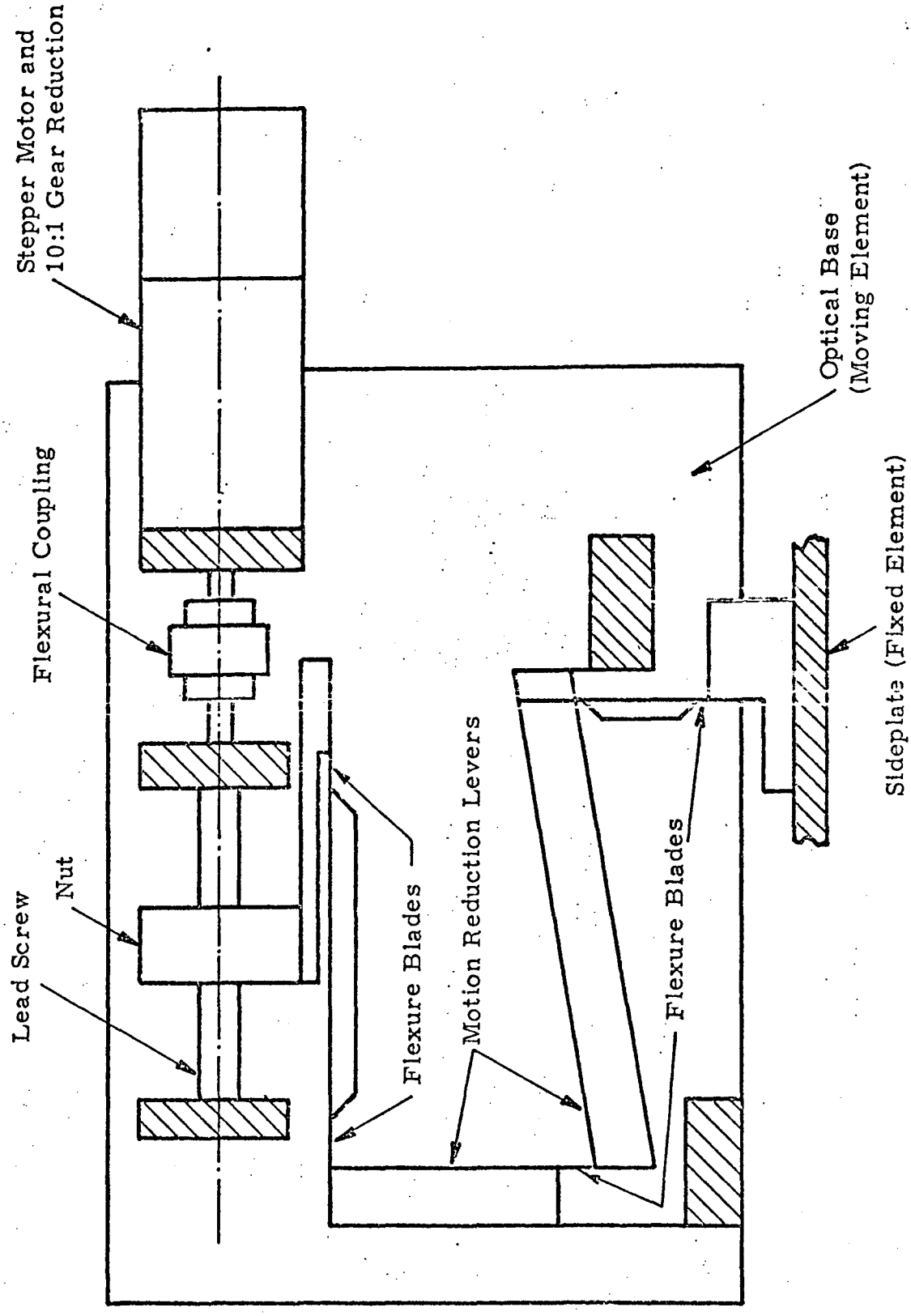
Stepper Motor and
10:1 Gear Reduction
Flexural Coupling
Lead Screw
Nut
Flexure Blades
Motion Reduction Levers
Flexure Blades
Optical Base
(Moving Element)
Sideplate (Fixed Element)

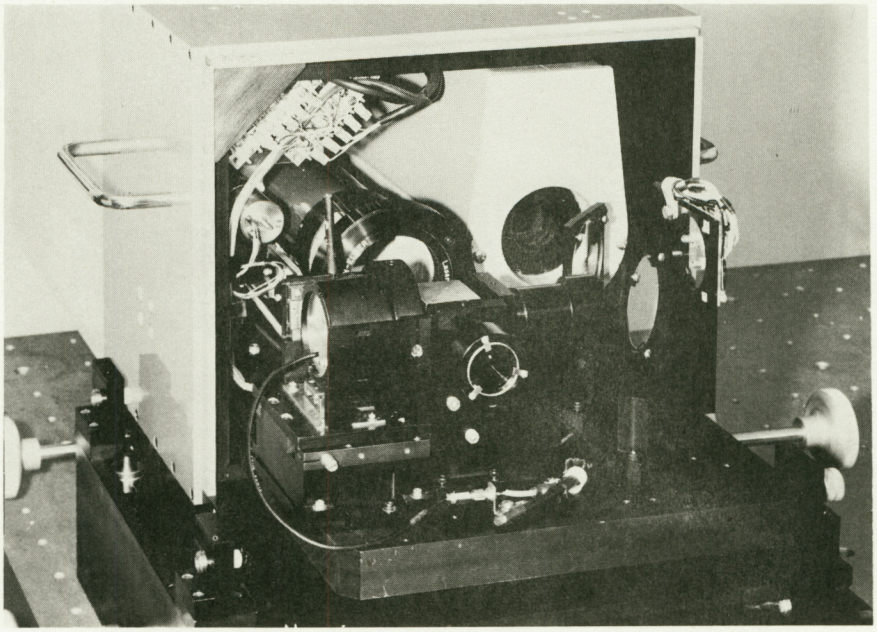

(a)

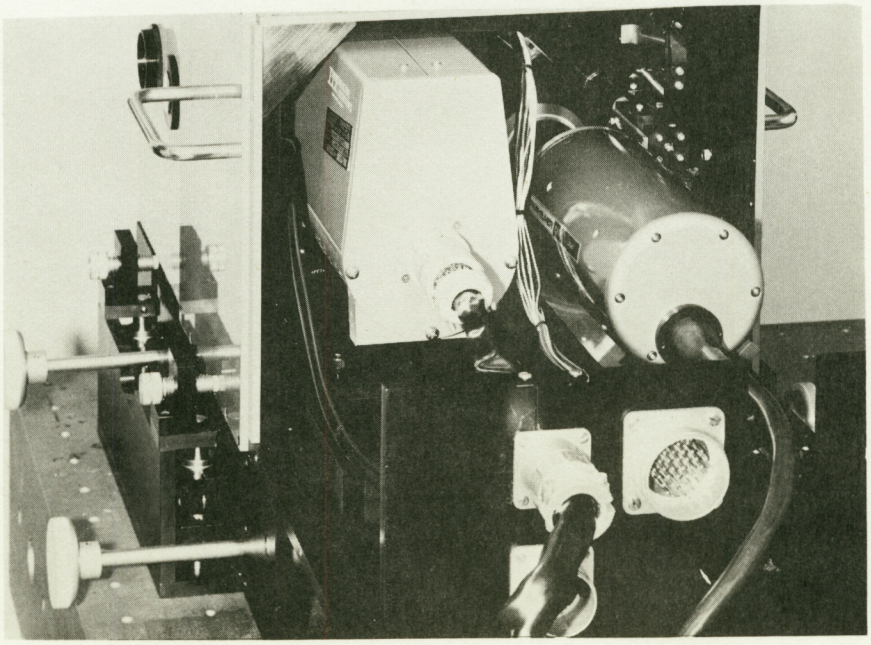

(b)

Figure 7. Optical Base

2.1.4 Doppler Frequency Shifter: The Doppler frequency shifter used during Phase I* was replaced by a Lansing piezoelectric translator model 21924 modified for positive voltage, capable of expanding five microns for an applied voltage of 1000 volts.

The operating triangular sweep frequency of the Doppler frequency shifter is 18 cycles/second.

2.2 SIGNAL PROCESSING ELECTRONICS

The figure sensor signal processing electronics, shown in the system block diagram of Figure 2, includes:

- Thermal compensating mount closed-loop electronics
- Image dissector output error detector and scanning electronics
- Doppler frequency-modulation electronics
- Power supplies
- Console instrumentation.

2.2.1 Thermal Compensating Mount Closed-Loop Electronics: The tilt angle signals used eventually to command the thermal compensators are derived by a pair of photodiodes located in the interferometer fringe pattern. The diodes are situated in the fringe pattern at a moment arm about the tilt axis of the test mirror as imaged at the fringe pattern. Three diodes are required for two tilt axes where one is a common (reference) diode, as illustrated in Figure 2. The photodiodes sense the test mirror tilt angle by measuring the optical phase shift that occurs across the mirror when it is angularly misalined with respect to the spherical reference mirror. These optical phase

* Refer to Final Report NAS 12-681, Section 3.0 (Ref. 1).

shifts are converted into DC output voltages by phase detector circuits and fed to the stepper motor drivers.

A "threshold" feature is used to automatically turn off the stepper motor in both axes whenever the mirror tilt errors have been nulled. This technique avoids limit cycling. As the mirror tilt errors increase above selected threshold levels, the actuator servo loop automatically becomes active to again nullify these errors.

The thermal compensator drive amplifiers sequence pulses (28 Vdc) into the stepper motor of the actuator. Each pulse results in a single step on the order of one third microinch displacement of the mount. The amplifier drives the actuator at five steps per second.

Because of the ambiguous output signal of the phase detector circuits whenever errors exceed ± 1/8 or ± 1/4 fringe*, coarse alignment is required to initially place the diodes within the correct (uniphase) operating range. This is accomplished by using the image dissector. The image dissector signals are fed into the thermal compensators while the 0.015-inch aperture is allowed to slowly scan from the projected reference diode point on the mirror to the adjacent diode point on the mirror in a given axis. As the image dissector scans, the actuators correct the tilt error at a rate proportional to the accumulated error across the mirror.

The controls for the two thermal compensators are located on the front panel of the control console as shown in Figure 8. Provisions have been made for selecting fine and coarse alignment, left and right slewing commands, and turning the actuators off.

2.2.2 Image Dissector Output Error and Scanning Electronics: The image dissector can measure the figure error of the test mirror, at any point, by scanning with a small 0.015-inch aperture. The dissector output signals are

* The phase detector output signals repeat every one fringe or 1/2 wavelength.

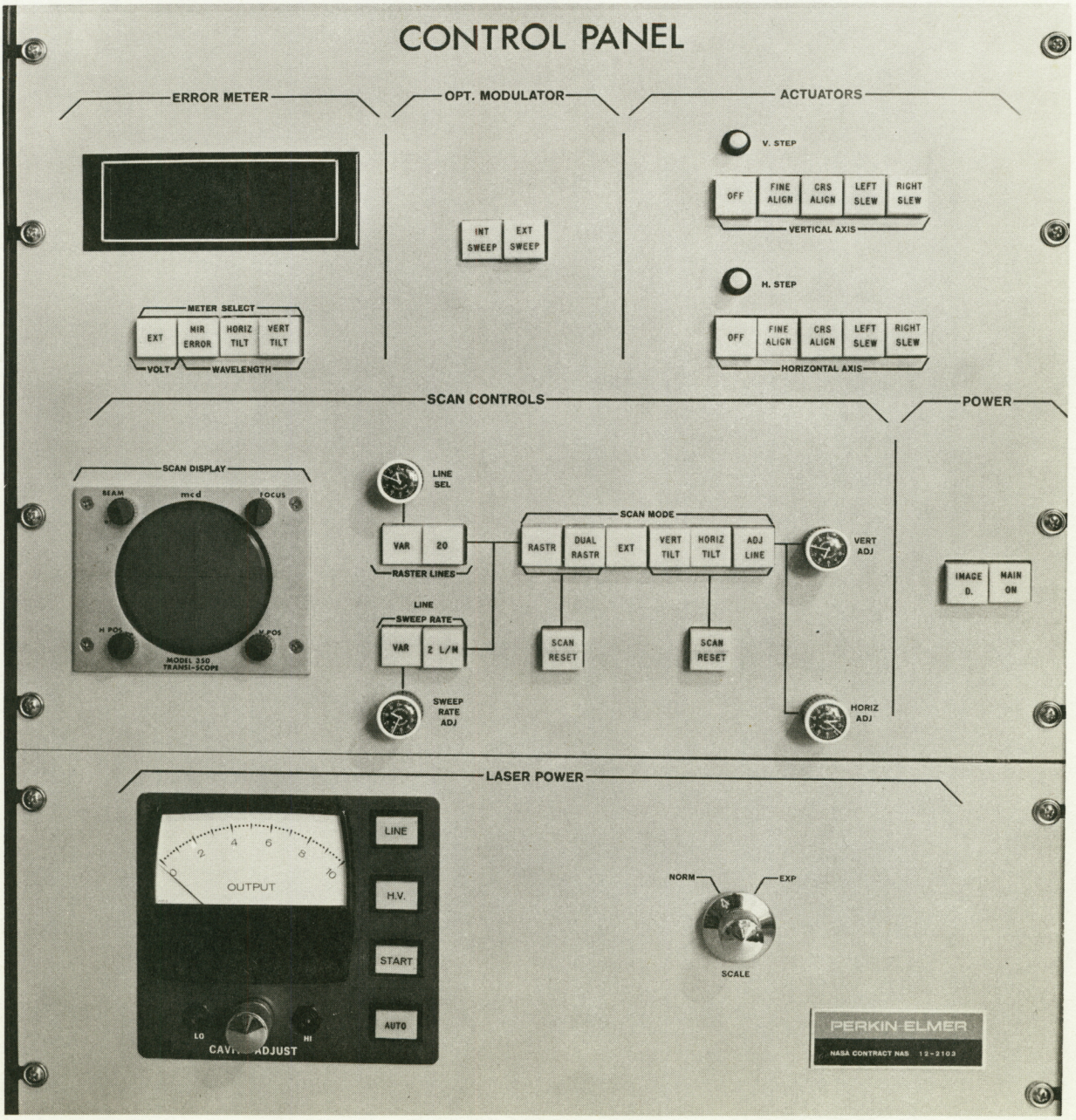

Figure 8. Console Front Panel

compared with the reference photodiode to determine the optical phase shifts, which are proportional to figure error. These phase shifts are converted into DC output voltages by a phase detector circuit similar to those used for the photodiodes.

Several scanning modes are used with the image dissector. The basic mode for measuring the error over the complete surface of the test mirror is a raster scan. During a raster scan the image dissector 0.0015-inch aperture sweeps horizontally across the fringe pattern (left to right), drops vertically downward by a small increment, again sweeps horizontally across the fringe pattern (right to left). It continues this process until the entire fringe pattern has been scanned. Digital/analog circuits are used to generate the raster scans. A digital "staircase" type generator is used to drive the deflection coils of the image dissector to accomplish vertical incremental steps and an analog triangular wave generator is used to drive the deflection coils to achieve the horizontal sweeps. The raster scan circuits were designed with both a fixed line (20) and a fixed sweep rate (2 lines/minute) control, and also a variable line and sweep rate control. The raster scan controls are located on the console front panel as shown in Figure 8. A "dual line" raster scan feature has also been included in the electronic design. This feature enables the image dissector aperture to automatically retrace each line for repeatability measurements.

Single line horizontal and vertical sweeps are used for coarse alignment of the thermal compensating mount, i.e., to achieve a uniphase fringe pattern. An analog sweep generator was designed for this purpose and an operational integrating amplifier. This same analog scanning generator is also used to equip the figure sensor electronics with an "adjustable line" scan feature. The adjustable line switch (Figure 8) allows an operator to set the image dissector scanning aperture to any point on the aperture of the test mirror where it will dwell as long as desired. An automatic single line scan can also be initiated to sweep from the reference diode to the selected point.

Finally, provisions have been made to bring in external scanning signals to the console via a test box, which feeds into a rear connector on the console. A front panel switch has been provided for this purpose in the bank of scan mode select switches.

2.2.3 Doppler Frequency Modulation Electronics: An analog triangular wave generator is used to derive the triangular waves that are fed to the high voltage piezoelectric drive amplifier. The triangular wave generator is the same one that was used during Phase I*, but the high voltage amplifier design was developed during this phase of the contract. It is a solid-state transistorized amplifier capable of producing output voltages up to 1200 Vdc at frequencies of 1 KHz, or greater, operating into capacitive type piezoelectric loads. This high voltage amplifier drives the piezoelectric element located in the Doppler frequency shifter at a frequency of 18 Hz over 10 fringes, which result in a carrier frequency of 180 Hz.

Front panel switches (INT. SWEEP, EXT. SWEEP), are located on the console to initiate Doppler frequency modulation either from internal drive or from external sweeps fed from other types of generators.

2.2.4 Power Supplies: The figure sensor power system is completely self-contained requiring only 115 Vac, 50/60 Hz input power. All DC power supplies are solid-state, of modular construction, regulated, and consist of the component parts listed in Table I.

All power supplies are located in the control console, including the Perkin-Elmer 5800 laser power supply and the ITT image dissector power unit. The controls for the laser power supply are located on the console front panel. The image dissector power unit is controlled by a single front panel switch. Similarily, all the DC power supplies are turned on by a single front panel switch which actuates several relays to supply 115 Vac, 60 Hz to all power units.

* Refer to Final Report, Advanced Figure Sensor, Figure 2.

TABLE I

POWER SUPPLY UNITS

Unit	Application
+15 Vdc	Operational Amplifiers
-15 Vdc	Operational Amplifiers
+12 Vdc	Digital Circuits
-6 Vdc	Digital Circuits
+5 Vdc	Digital Circuits
+28 Vdc	Relay Voltage
+1380 Vdc	Laser Frequency Modulation Amplifier
+400 Vdc	Peristaltic Actuator Amplifiers
+28 Vdc	Stepper Motor

2.2.5 Console Instrumentation: In addition to the front panel switches which control power, scanning modes, thermal compensators, and the optical modulator, a 3-1/2 digit digital error meter and a 3-inch oscilloscope have been incorporated into the design of the figure sensor electronics. The digital error meter can be selected to read (1) the mirror figure error (i.e., output of the image dissector phase detector circuit, (2) the photodiode vertical and horizontal phase detector circuits output signals, (3) external voltages fed through the console test box and (4) voltages which indicate the position of the thermal compensation actuators within their range. The 3-inch oscilloscope is permanently connected to monitor the signals going to the vertical and horizontal deflection coils of the image dissector. The oscilloscope therefore visually displays the scan modes.

3.0 PERFORMANCE EVALUATION

The test results, test procedures, and test set-ups for the working model of the advanced figure sensor are discussed in the following paragraphs.

3.1 TEST SET-UP AND CALIBRATION OF OPTICAL ELEMENTS

During the early stages of testing, two major problem areas were encountered that required a refinement in the test set-up for the figure sensor. First, vibrations were excessive, causing large optical output errors at the fringe pattern. The figure sensor assembly and test mirror were originally mounted on a 6x3x1/2 foot steel table, which was supported on isolation pads. In this set-up, building vibrations were not sufficiently isolated and the figure sensor assembly and manual adjustment stand were constantly subjected to these external disturbances. The adjustment stand was particularly susceptible to external vibrations even though it was designed to be rigid with all bearings and adjustments properly preloaded. Locking screws were therefore added to secure the mounting base of the adjustment stand to the figure sensor baseplate or (main outer frame) to increase the rigidity of the stand once the correct stand position was achieved. The largest improvement, however, was obtained by replacing the isolation pads with pneumatic vibration isolators built by Barry Controls. The pneumatic isolators were capable of isolating the steel table from external disturbances with frequencies of 1/2 Hz and up. A photograph of the test set-up is shown in Figure 9.

The second problem encountered was air turbulence which caused varying path length changes between the mirror and figure sensor assembly. The turbulence was minimized to acceptable levels by simply using an enclosure that covered the test mirror and figure sensor assembly.

All testing was done in a small, dark room, approximately 10x10x8 feet. Room temperature (68°F) prevailed during testing, extending slightly higher at times since air flow into and out of the room was minimized

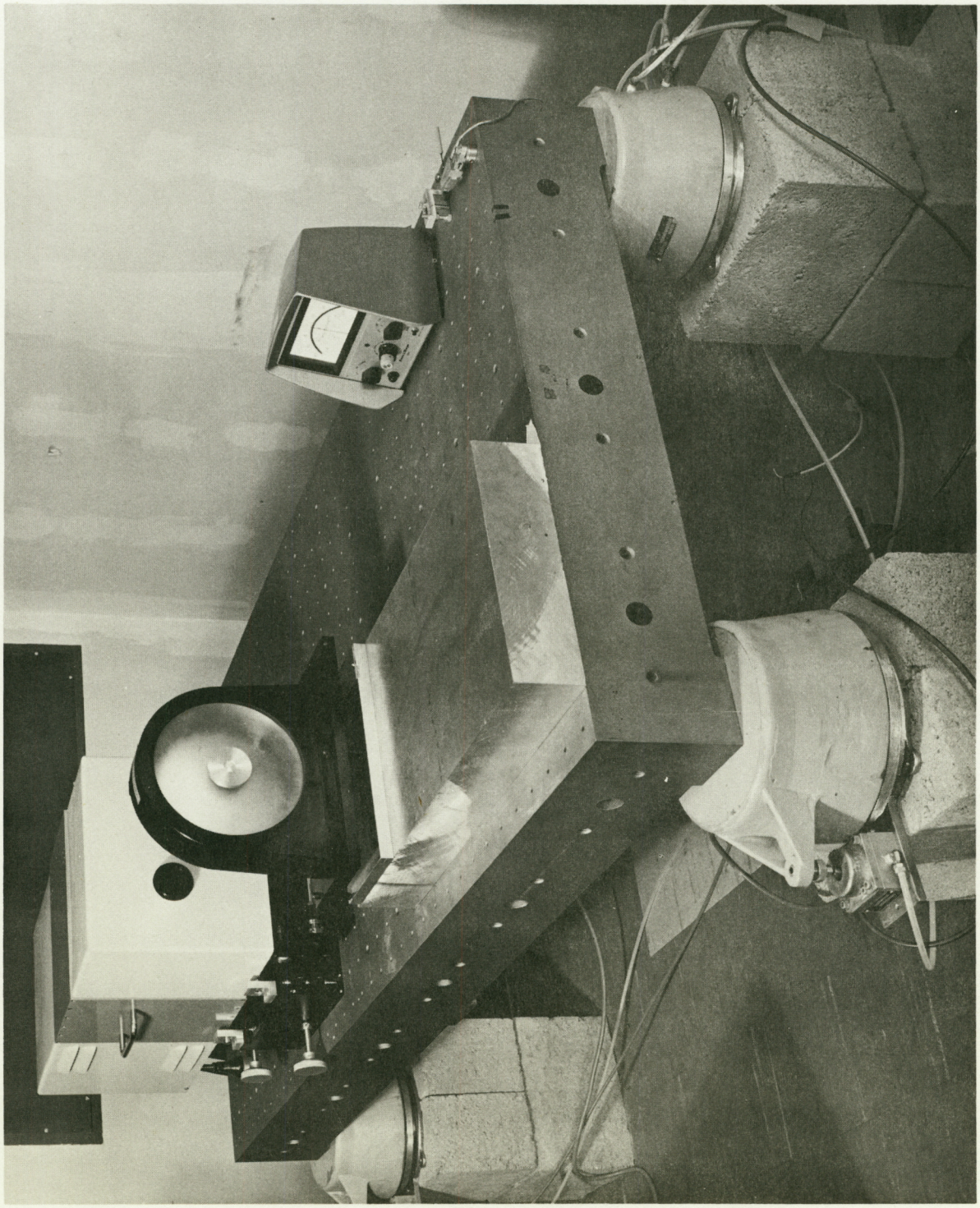

Figure 9. Figure Sensor Test Set-up

3.2 TEST RESULTS

3.2.1 Thermal Compensation Actuators: The thermal compensating mount was tested in both axes in open and closed loop operation. Open loop tests consisted of slewing the thermocompensator in the forward and reverse directions while monitoring the photodiode phase detector outputs to determine figure sensor displacement and rates based on fringe count. A sample test run is shown in Figure 10. The data was recorded with a two channel Sanborn recorder. The top trace of Figure 10 is the image dissector phase detector output and the bottom trace is the horizontal axis photodiode phase detector output. The horizontal actuator was placed in a slewing mode so that traces of Figure 10 represent fringes cycling every 1/2 wavelength. Each chart line is 1mm. A complete cycle is one fringe or $1/2\lambda$. The calibration, based on the lines drawn to coincide with the slope of the fringe through null or zero error is 24 cm/λ (image dissector) and 20 cm/λ (photodiodes).

An angular tilt displacement to produce an optical path difference of $\lambda/2$ (one fringe) is equivalent to a lateral displacement of 0.000062-inch at the center of curvature of a f/2.5 spherical test mirror and at a frequency of $\lambda = 6328\text{Å}$. The number of fringes counted as a function of lateral displacement was three for a slewing time of 60 seconds. Thus the thermal mount average slewing rate is equal to

$$\frac{0.000062 \times 3}{60 \text{ sec}} = 3 \times 10^{-6} \text{ inch/sec}$$

Typical closed loop operation of the actuators is shown in Figure 11. For this test, the horizontal actuator was placed in the slewing mode for an arbitrary period of time and then switched into the "fine alignment" mode. The point at which the fine alignment mode was initiated is noted on the traces. In the fine alignment mode, the actuators are in a closed loop configuration receiving signals from the photodiodes. The error is quickly reduced and remains near zero once the servo loop has been closed.

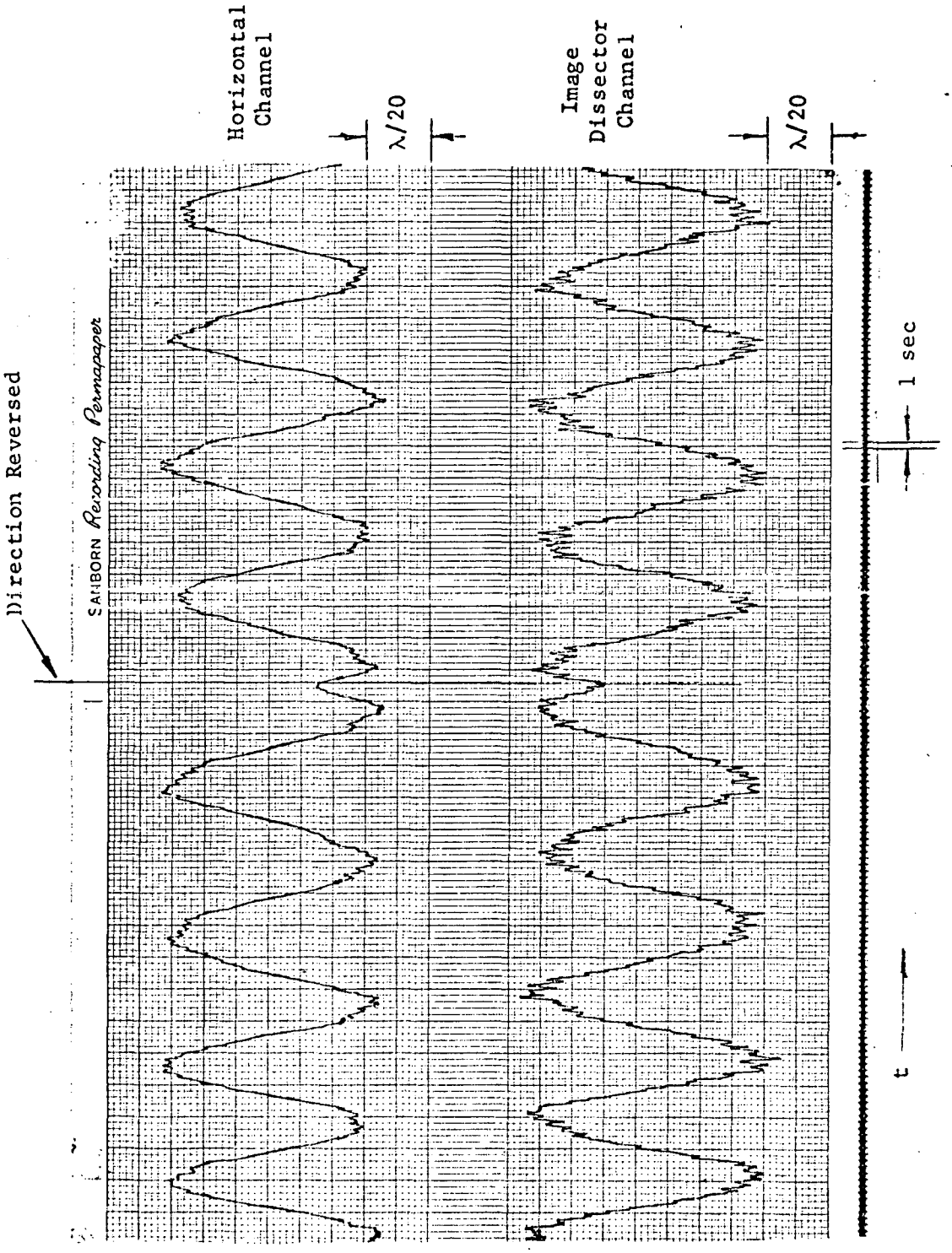

Figure 10. Open Loop Slewing Measurement

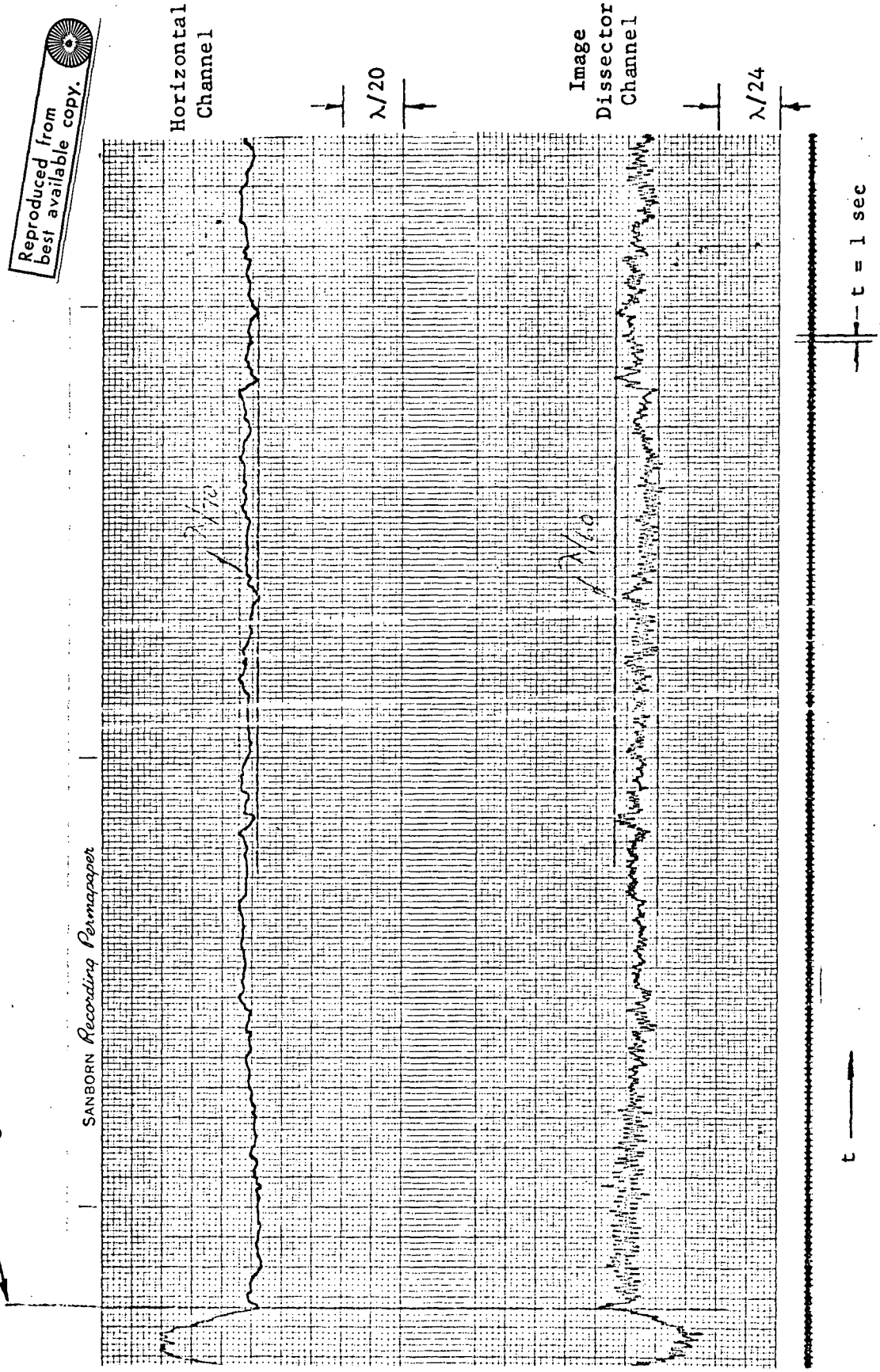

Figure 11. Closed Loop Control

3.2.2 Stability Measurements: Stability measurements were made in both the vertical and horizontal photodiode channels and also in the image dissector channel. Sample test runs are shown in Figures 12, 13, and 14. Figure 12 is typical data samples of the horizontal (upper trace) and vertical (lower trace) photodiode phase detector outputs taken 15 minutes from the time the fine alignment of the thermal mount mode was initiated. These are worst case samples taken during excessive external disturbance conditions. Peak variations were up to 2.5 chart lines. The calibration is 20 cm/λ where each chart line is 1mm. 2.5 chart lines result in a peak error of $\lambda/80$ with rms values on the order of $\lambda/200$ using a 2.5 peak-to-rms ratio.

The lower trace of Figure 13 is a sample plot of the image dissector phase detector output measured at horizontal tilt position. The recorder gain is set to give a scale of 80 cm/λ. The upper trace of Figure 13 is the horizontal diode phase detector output. Figure 14 shows the image dissector and diode phase detector outputs for the vertical control channel. The samples were taken at ten minutes into the runs. The image dissector stability errors were $\lambda/50$ peak or less near the null position. The photodiode channels stability were $\lambda/80$ peak.

3.2.3 Resolution Measurement: The resolution of the figure sensor was measured by a "knife edge" type test conducted as follows. A slit, 0.100 inch wide, was fastened across the aperture of the image dissector. The image dissector was commanded to slowly scan in the horizontal direction across the mirror aperture and across the slit. The image dissector output signals were recorded, as shown in Figure 15, to obtain a measurement of the time required to reduce the signal from maximum to zero (or vice versa) as the spot traveled over the edges of the slit. Since the scanning rate was constant and the slit width was known (0.100 inch) and provided edge marks (i.e., signal drops to zero at the edge of the aperture), the dissector aperture displacement versus time was established. The small scanning aperture traveling across an edge of a slit exhibits a steady decrease or increase in signal. The time interval for the signal to go from one extreme to another determines the slit aperture. Referring to Figure 15A to B, 430mm long, the time axis

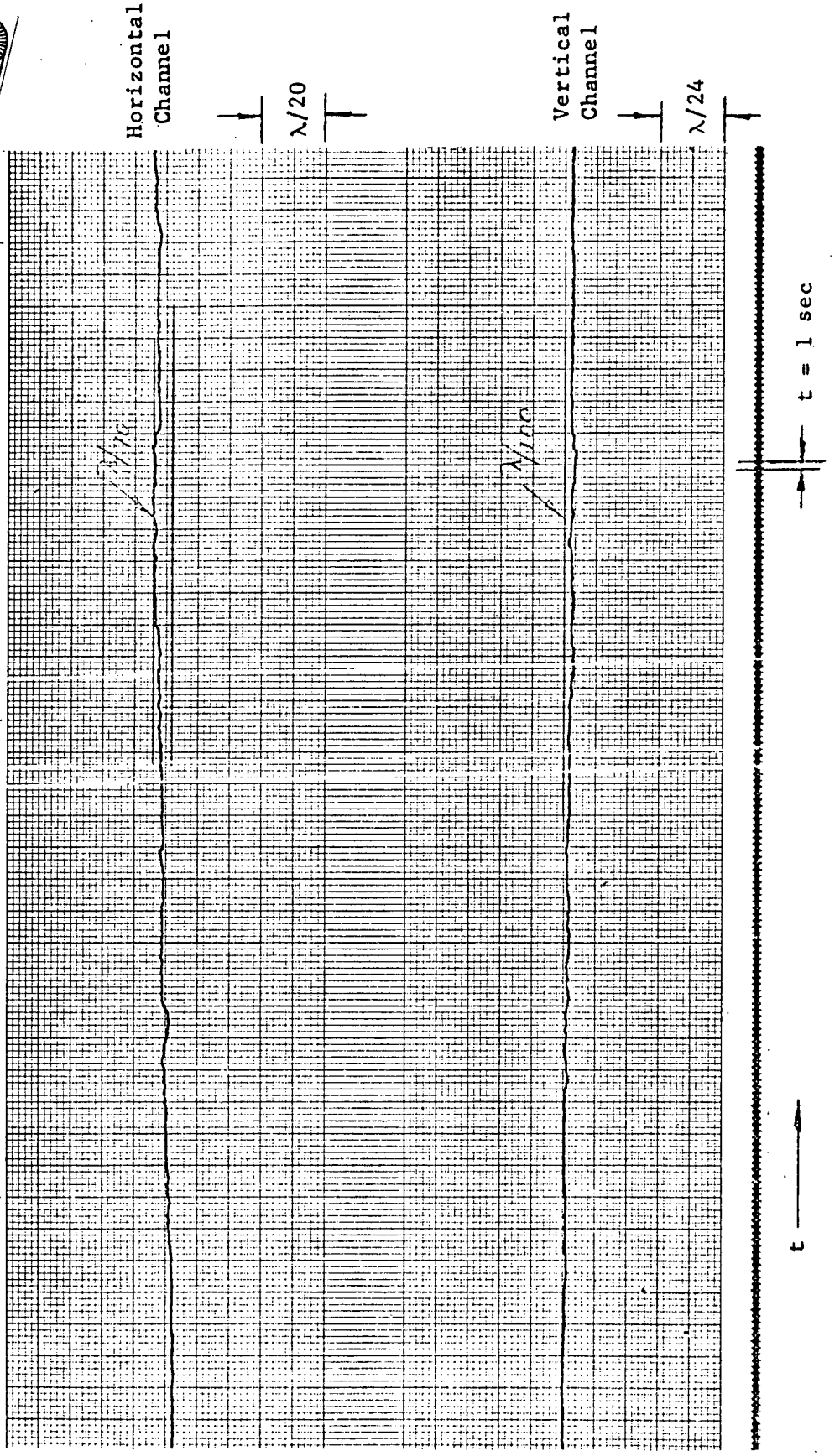

Figure 12. Stability Measurement

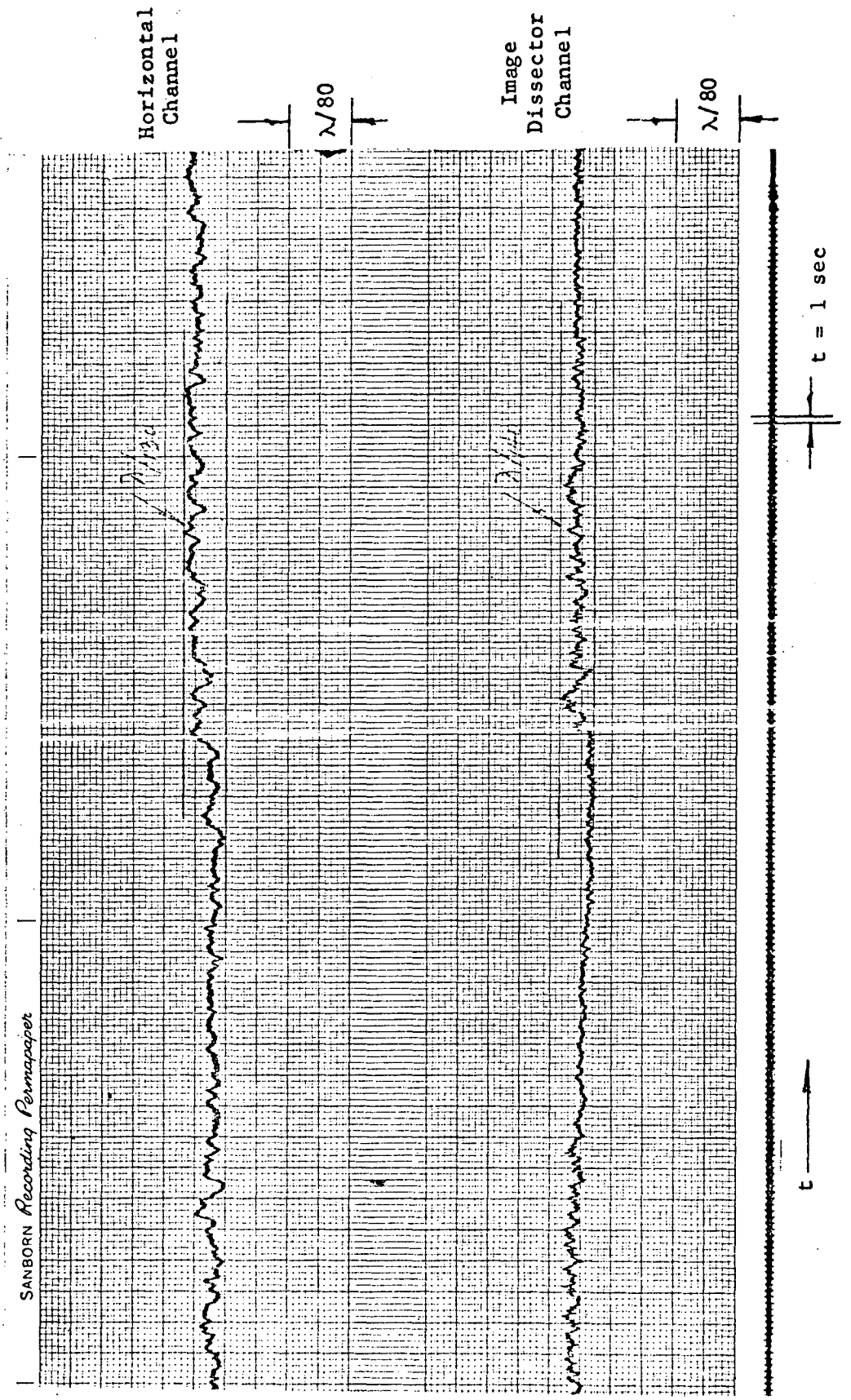

Figure 13. Closed Loop Stability Test

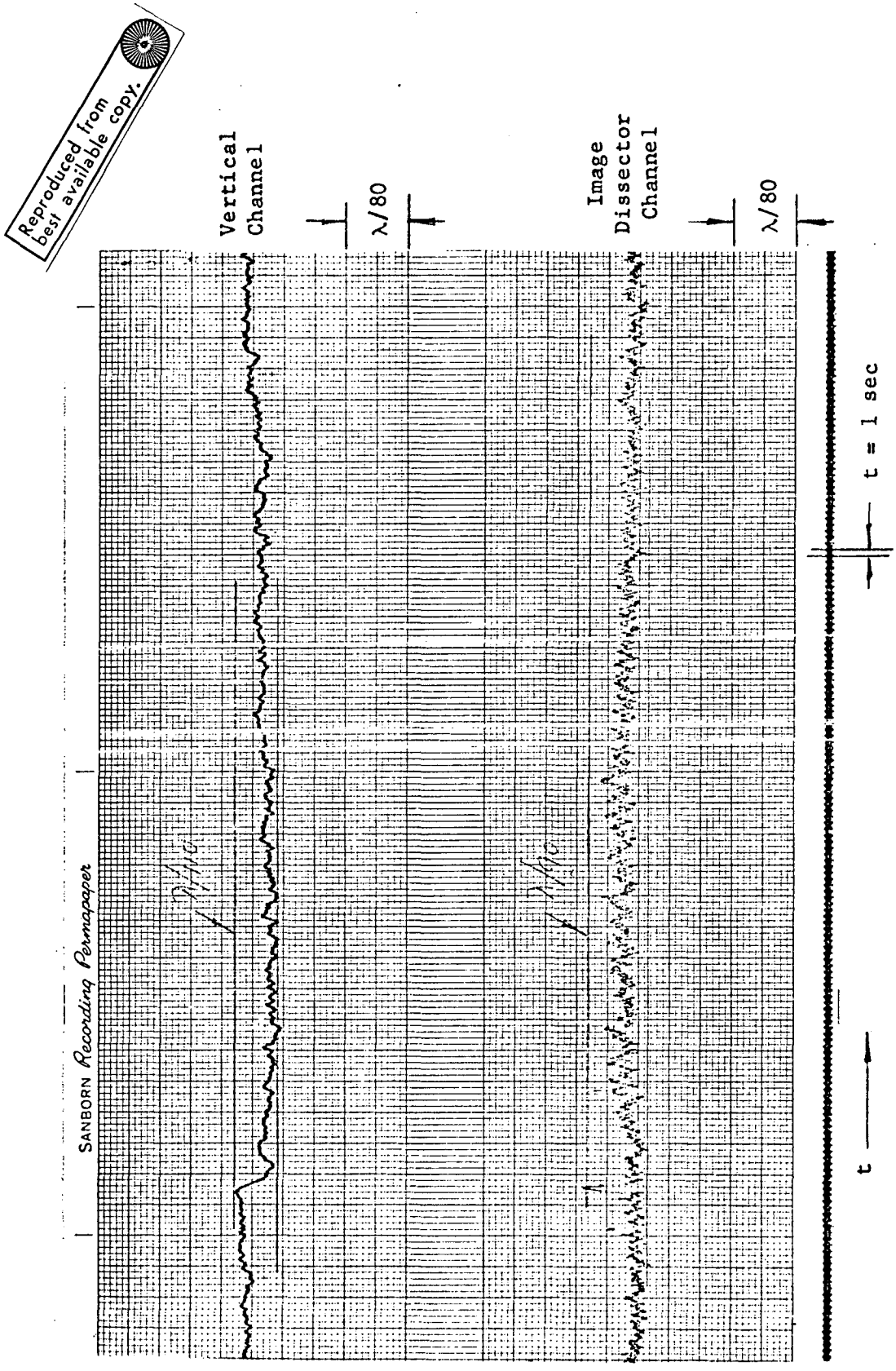

Figure 14. Closed Loop Stability Test

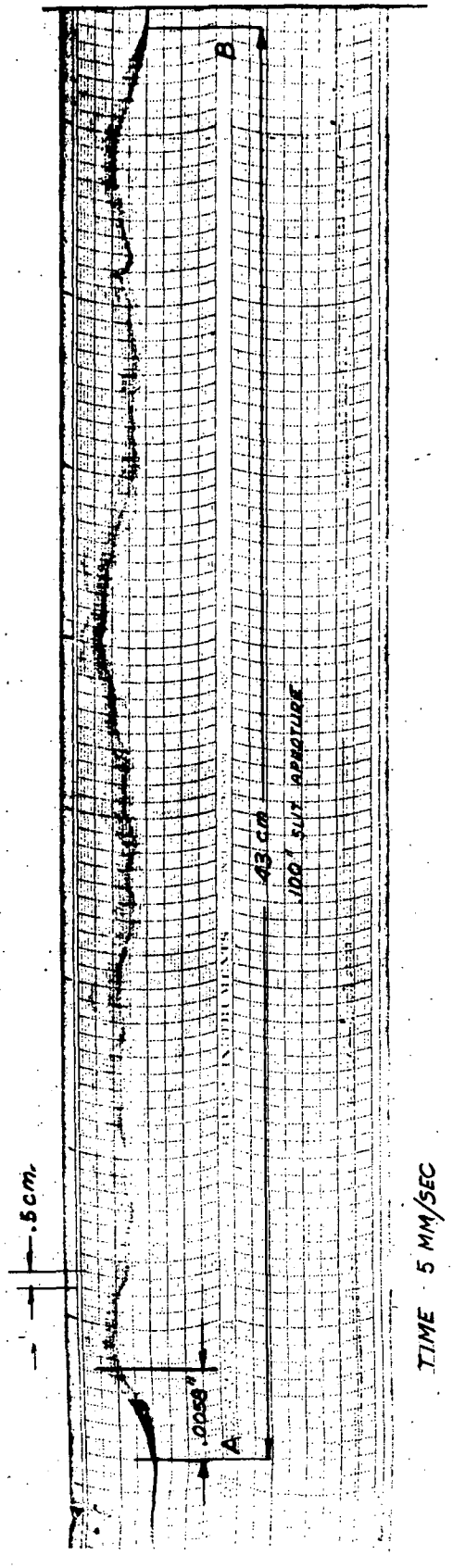

Figure 15. Resolution Measurement

represents 0.006-inch at the image dissector. Repeated measurements established the signal "turn on" time interval at 2.5mm or 0.006-inch, which is the aperture diameter. This value was higher than the 0.0015-inch specified by the vendor (ITT). An aperture of 0.006-inch, however, is the equivalent of 145 fringes across the mirror, which meets the "100 fringe" resolution requirement for the figure sensor. The 145 fringe value is arrived at as follows. The clear aperture of the test mirror is reduced to an image size of 22.5mm, or 0.88-inch, at the image dissector. Dividing the image size of 0.88-inch by 145 results in an overall fringe spacing of 0.006-inch.

3.2.4 Raster Scans: Numerous raster scans were obtained for the figure sensor to determine the optical errors in the system. The calibration in volts per wavelength remains constant over the entire mirror aperture. A scanning rate of one line/30 seconds was used during all raster measurements except for those tests deliberately conducted at faster scan rates to determine system response. A 7000 x-y Hewlett-Packard recorder was used for all the measurements.

Prior to raster scan measurements, the calibration was established for the 7000 x-y Hewlett-Packard recorder at one inch = $\lambda/8$. Figure 16 gives plots of calibration runs for the entire aperture. Appropriate lines have been drawn coincident with the fringe slopes to establish the theoretical peak output voltages. These calibration runs were obtained by setting a tilt error of a few fringes and scanning with the image dissector.

The system was aligned to achieve minimum error or fringes and raster scans were made as shown in Figures 17, 18, 19, and 20. The thermal mount was active during these tests, operating in the fine alignment closed loop mode. The system was coarse aligned to less than $\pm$ 1/4λ prior to engaging the fine alignment mode.

During each raster scan, an automatic timer periodically resets the image dissector channel output to zero as shown in Figure 17. This reset feature permanently records the point of zero error.

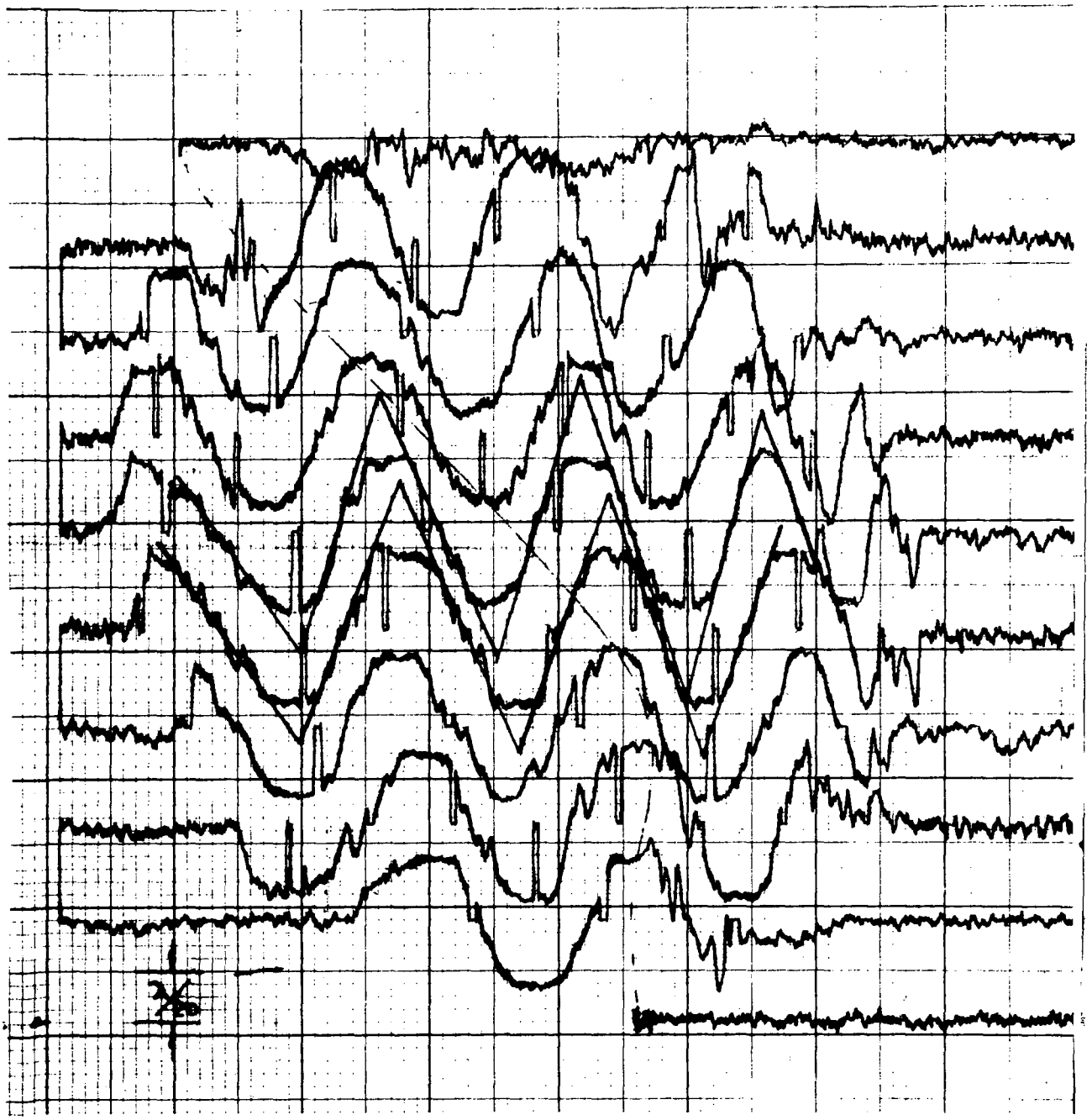

Figure 16. Raster Scan Calibration

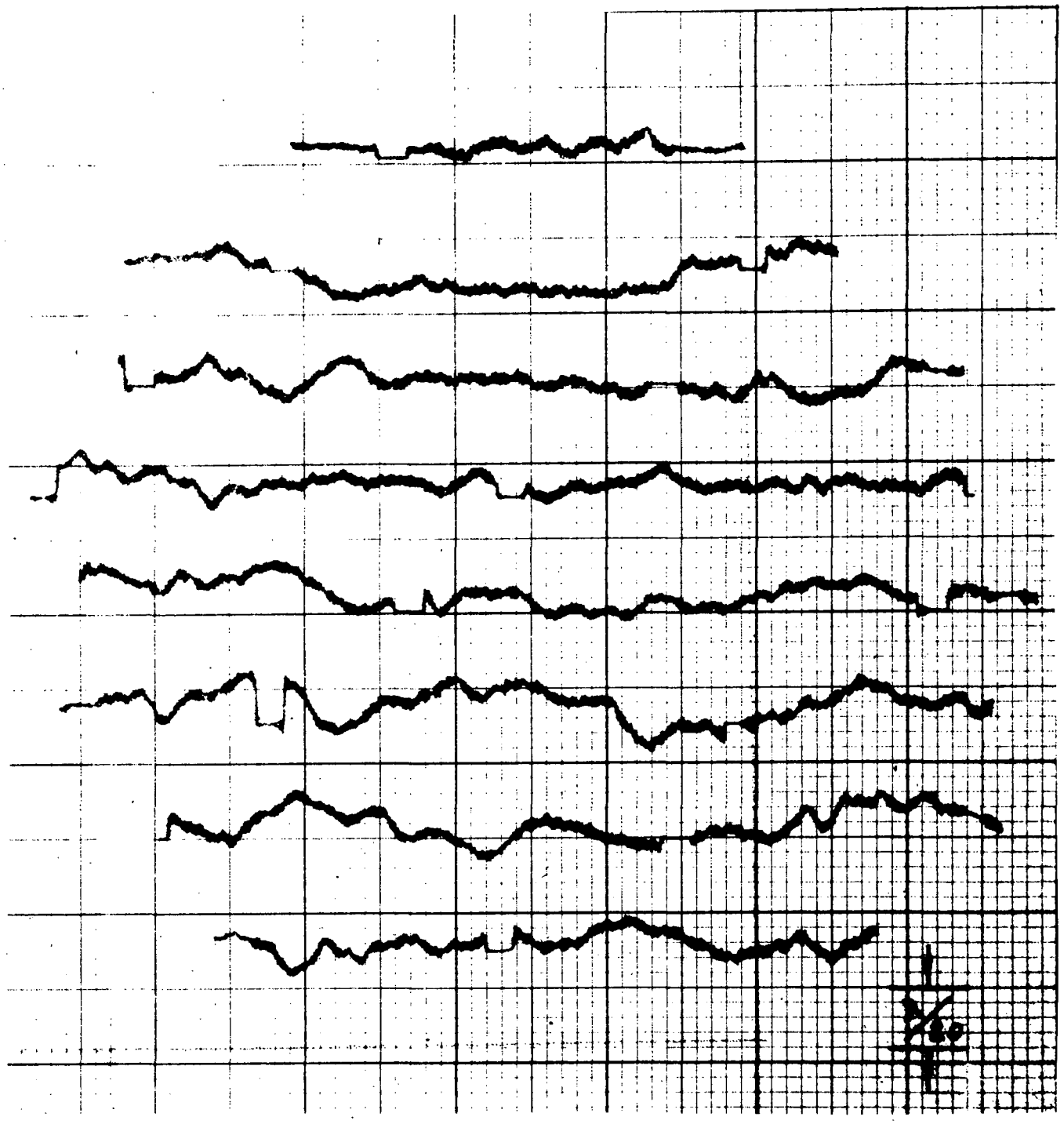

Figure 17. Raster Scan of Test Mirror Showing Figure Error of Interferometer

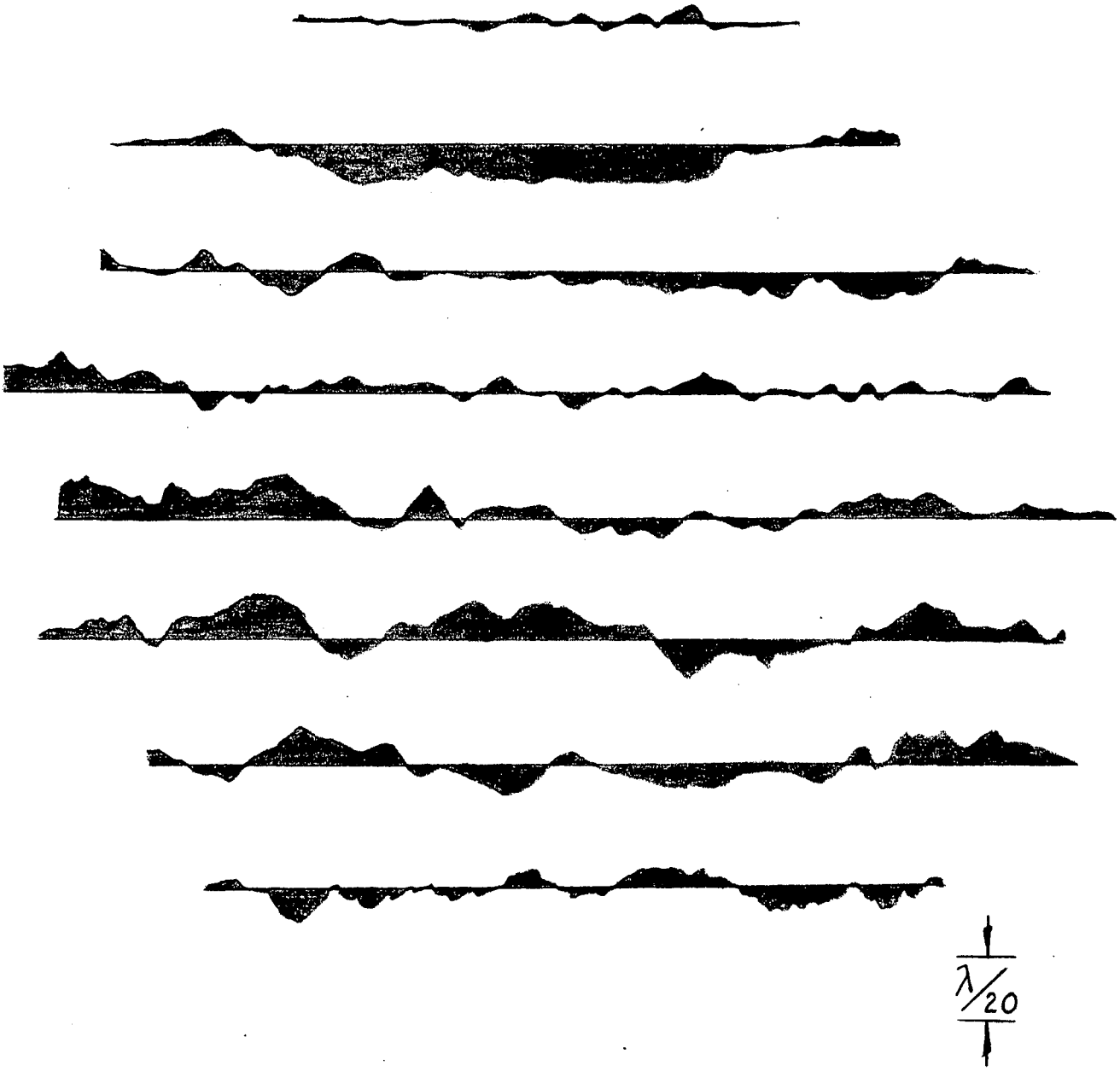

Figure 18. Profile of Interferometer Error Component Made From Raster Scan of Figure 17

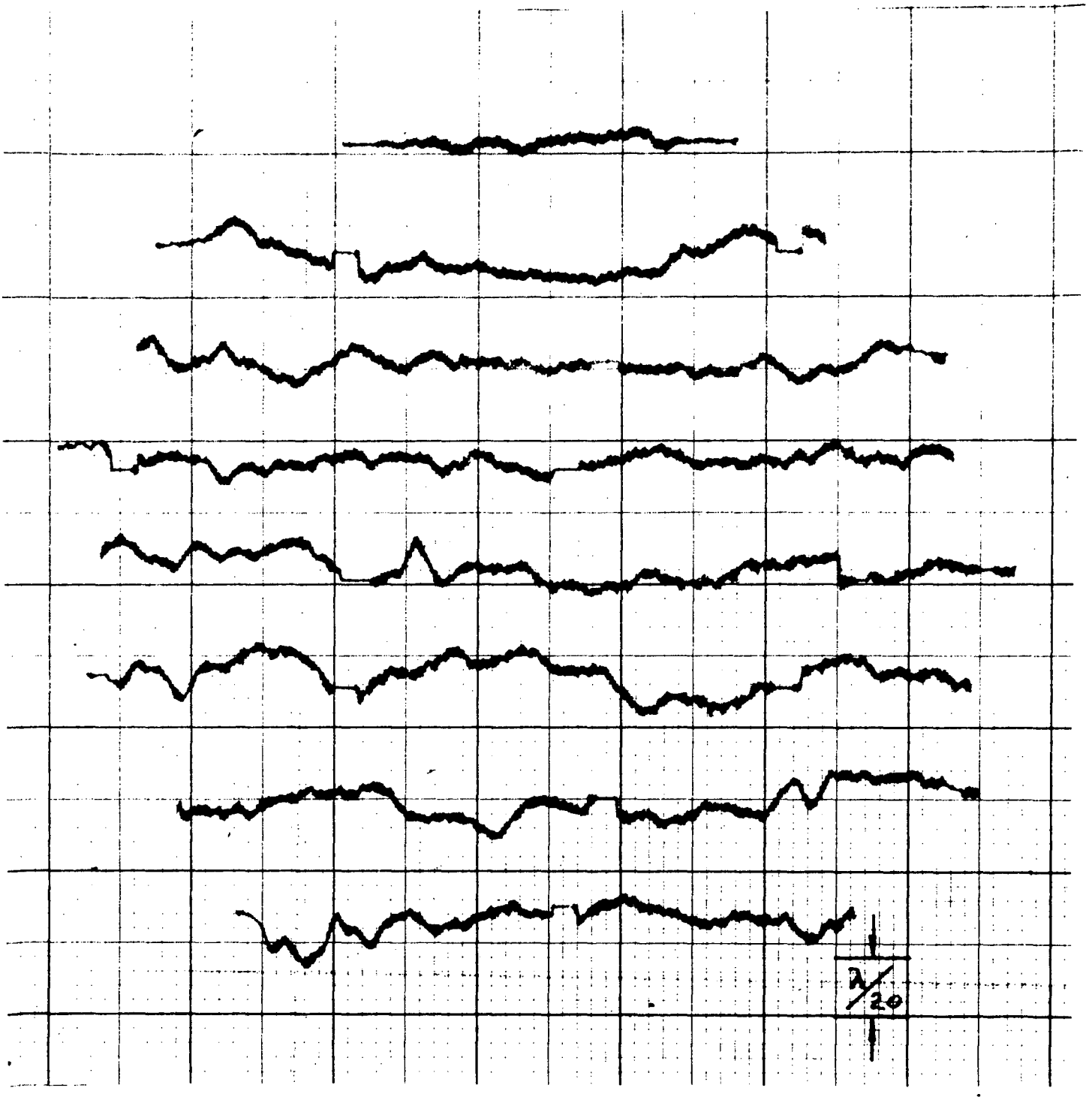

Figure 19. Raster Scan After Realignment of Interferometer

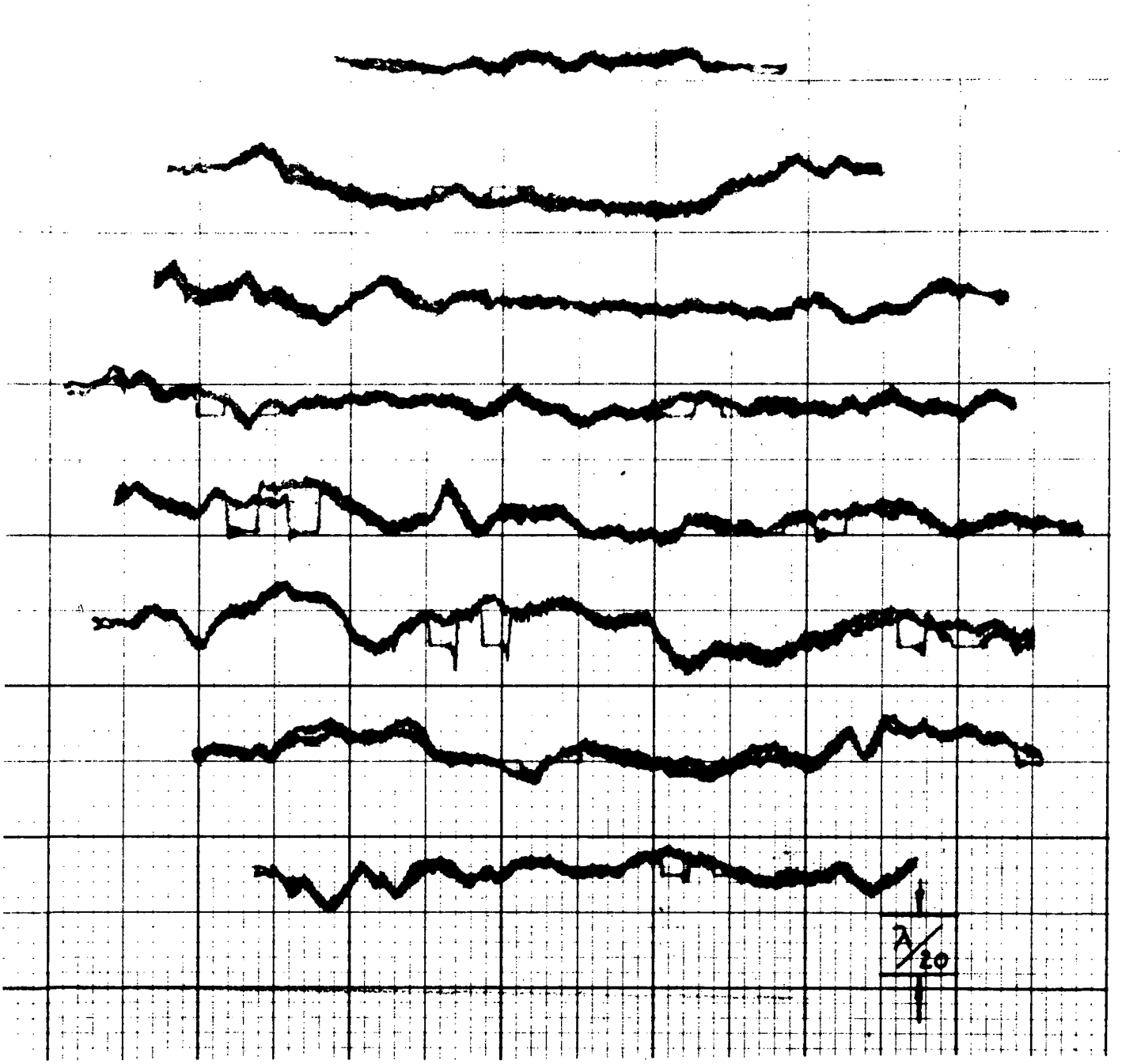

Figure 20. Double Raster Repeat Scans to Demonstrate Control System Stability

In Figure 18 the areas between the scans and the zero baseline, which represents a best fit sphere, have been filled in to show the error profile more clearly. A maximum peak to peak error of $\lambda/16$ is observed in Figure 18 and the rms value of the error introduced by the interferometer as measured from Figure 18 is approximately $\lambda/80$. Rotational and lateral displacement of the decollimating lens did not appreciably affect the figure scans so it is concluded that most of the error observed comes from the 32mm cube beamsplitter, which has 7 surfaces that could contribute to the cumulative error.

The figure sensor was completely realigned to again achieve minimum figure error across the aperture of the mirror and the resulting scans are shown in Figure 19. The errors are almost identical to those of Figure 17.

Figure 20 shows the result of repeating the raster scans after an interval of approximately 20 minutes. The maximum difference at any point is $\lambda/80$ which confirms the stability measurements of paragraph 3.2.1.

It was clearly noted during repeatability tests that external disturbances were the cause of large excursions. To achieve good repeatability results, it was necessary to stabilize air turbulence as much as possible and carefully avoid physically disturbing the figure sensor and mirror during test runs.

3.2.5 Interferogram: Figure 21 is an interferogram taken at the output of the interferometer, using the beam divider which was added to the assembly to permit visual or photographic evaluation of the interference pattern in the mirror image. The test mirror is translated laterally from the aligned position to give a straight line fringe pattern.

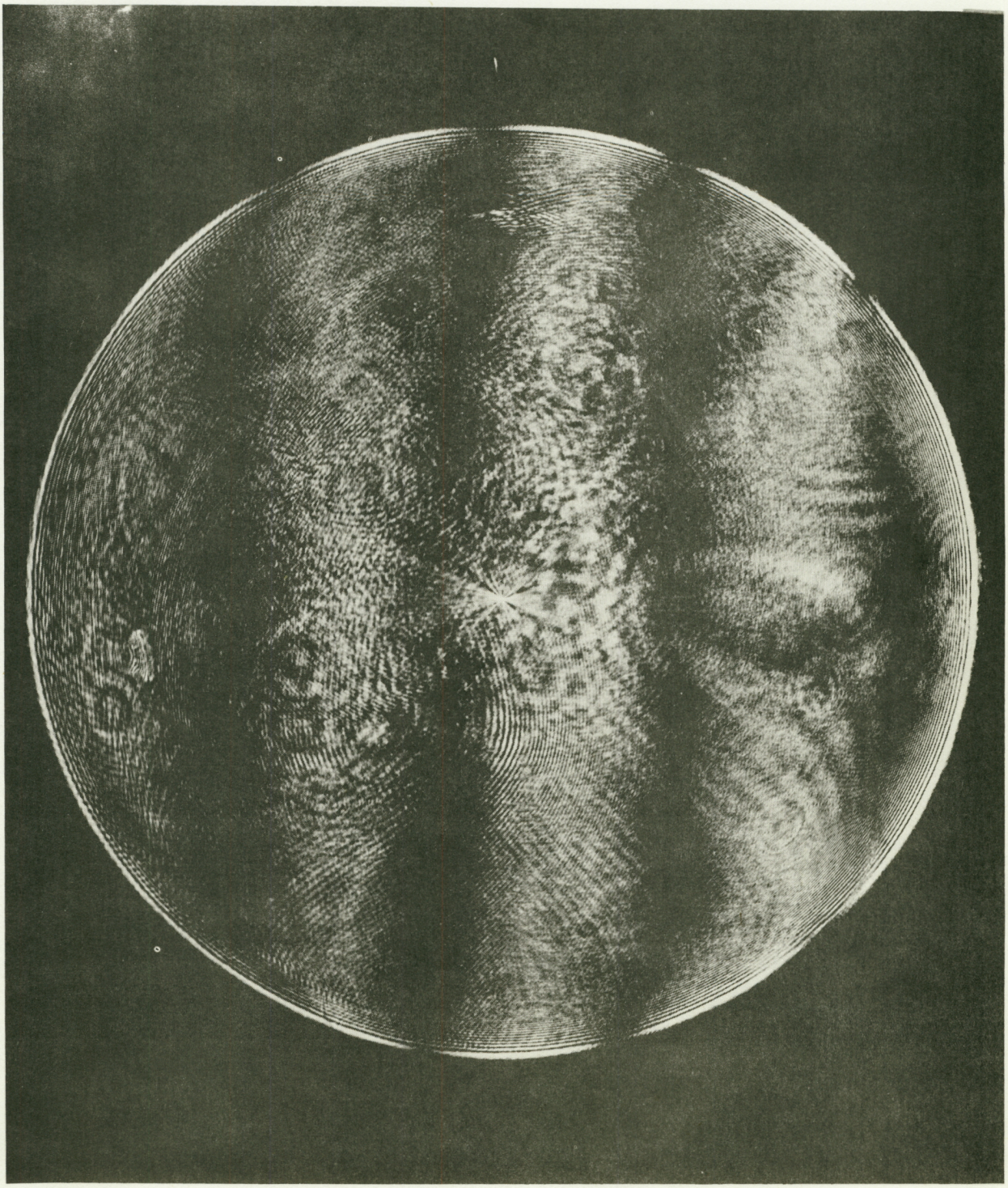

Figure 21. Interferogram with Test Mirror